Available online at www.sciencedirect.com
ScienceDirect
Geochimica et Cosmochimica Acta 73 (2009) 7341–7359
Geochimica et Cosmochimica Acta
www.elsevier.com/locate/gca

Liquid composition-dependence of calcium isotope fractionation during diffusion in molten silicates

James M. Watkins [a,*], Donald J. DePaolo [a,b], Christian Huber [a], Frederick J. Ryerson [c]

[a] Department of Earth and Planetary Sciences, University of California, Berkeley, CA 94720-4767, USA
[b] Earth Sciences Division, Lawrence Berkeley National Laboratory, Berkeley, CA 94720-4767, USA
[c] Lawrence Livermore National Laboratory, L-638, LLNL, Livermore, CA 94550, USA

Received 13 January 2009; accepted in revised form 2 September 2009; available online 15 September 2009

Abstract

Liquid phase diffusion experiments were carried out to determine whether diffusive isotopic fractionation of a major chemical element (Ca) varies with chemical composition in high-temperature molten silicates. The objective was to determine how differences in silicate liquid structure, such as the ratio of bridging to non-bridging oxygen atoms, as well as bulk transport properties such as viscosity, relate to isotope discrimination during diffusion. This information, in turn, may relate to the lifetimes and sizes of multi-atom structures in the liquid. Diffusion couples consisting of juxtaposed natural mafic and felsic liquids were held at $T = 1450$ °C and $P = 1.0$ GPa for durations of 12–24 h in a standard piston–cylinder assembly. Experiments were done using different mafic endmember compositions (two tholeiitic basalts and a ugandite) and a single rhyolite composition. Major-element diffusion profiles and Ca isotope profiles were measured on the recovered quenched glasses. The starting materials were isotopically indistinguishable, but $^{44}Ca/^{40}Ca$ variations of ca. 5‰ arose due to a mass dependence of the Ca diffusion coefficients. Results indicate that the mass dependence of Ca diffusion coefficients varies with the magnitude and direction of aluminum gradients and the viscosity of the liquid. Some Ca fractionations result mainly from Al gradients.

A simplified multicomponent diffusion model was used to model the experimental results. The model allows for diffusion of Ca in response to gradients in the concentrations of both CaO as well as Al_2O_3, and the model results are consistent with the inferred existence of at least two distinct species of Ca. The magnitude of isotopic discrimination during diffusion also appears to be stronger on the rhyolite versus the basalt/ugandite side of diffusion couples. The results can largely be accounted for by an adaptation of the model of Dingwell (1990), whereby in high silica liquids, Ca diffuses largely by site hopping through a quasi-stationary aluminosilicate matrix, producing strong isotopic effects because the Ca diffusion is not strongly correlated with the movement of the framework atoms. In low-silica liquids, Ca diffusion is correlated with the movement of the other components and there is less mass discrimination. Combining our Ca results with Ca, Mg, and Li data from previous studies, we show that this model can explain most of the cation- and composition-dependence of diffusive isotopic fractionations observed thus far. A key parameter controlling isotopic discrimination is the ratio of the elemental (Ca, Mg, Li) diffusivity to the Eyring (or Si) diffusivity. However, all experiments done so far also exhibit isotopic features that are not yet fully explained; some of these may relate to small temperature gradients in the capsules, or to more complex coupling effects that are not captured in simplified diffusion models.
Published by Elsevier Ltd.

1. INTRODUCTION

Natural silicate liquids can be viewed as "concentrated solutions" of roughly ten major elements distributed among various dissolved chemical species. The nature of these dissolved species is of broad interest for understanding

* Corresponding author.
E-mail addresses: jwatkins@berkeley.edu (J.M. Watkins), depaolo@eps.berkeley.edu (D.J. DePaolo), chuber@seismo.berkeley.edu (C. Huber), ryerson1@llnl.gov (F.J. Ryerson).

0016-7037/$ - see front matter Published by Elsevier Ltd.
doi:10.1016/j.gca.2009.09.004

thermodynamic and transport properties of silicate liquids (e.g. Navrotsky et al., 1989; Ghiorso et al., 1983; Hess, 1995; Ghiorso et al., 2002; Halter and Mysen, 2004), and yet, it is difficult to define the actual chemical constituents in a melt because of the disordered and dynamic nature of silicate liquid structures. Our focus in this work is on the relationship between liquid structure and isotopic diffusion. In particular, we are interested in whether the relative mobility of isotopes reflects the relative mobility of isotopically-distinct complexes, and if so, how does this fit into the emerging picture of silicate liquid structure and dynamics?

1.1. Speciation and silicate liquid structure

The main structural units in silicate materials are silica and alumina tetrahedra that are either isolated or are linked together by bridging oxygen atoms to form chains, rings, sheets, and three-dimensional networks of $(Al,Si)O_x$ structural units (Calas et al., 2006; Henderson et al., 2006). In the liquid state, these aluminosilicate structures do not move as long-lived, well-defined molecular units, but are constantly reorganizing through rapid breaking and reforming of bridging oxygen bonds (Stebbins, 1995). The definition of chemical "species" in silicate liquids thus becomes ambiguous, since it depends on the interconnectivity as well as the longevity of aluminosilicate networks, and the strength with which the other cations (e.g., Fe, Mg, Ca, Na, K) are bonded to them. This ambiguity makes it difficult to parameterize the configurational entropy of silicate liquids and represents a major obstacle for producing an accurate general model for their thermodynamic properties (e.g. Hess, 1995; Ghiorso et al., 2002).

There is a long history of research on the molecular-scale structures of silicate liquids and glasses (see Mysen and Richet, 2005 for a recent synthesis). A variety of spectroscopic and diffraction techniques are used to probe structures in glasses and liquids, and each is sensitive to the structure at different length and time scales. X-ray scattering and absorption probe structures as they appear on timescales of about 10^{-16} s and the resulting spectra for a given element are sensitive to the local bonding environment up to length scales of about 10 Å (e.g., bond distance, bond angle, coordination number, and connectivity to the first few neighboring atoms; Brown et al., 1995). Vibrational spectra (e.g., Infrared and Raman) probe interatomic bonding environments averaged over timescales of about 10^{-12} s and have been used to identify chemical species with lifetimes greater than this value (McMillan and Wolf, 1995). Nuclear-magnetic resonance (NMR) methods probe local chemical environments up to about 10 Å over timescales ranging from 10^{-4} to about10^{-8} s (Stebbins, 1995). The timescale relevant for diffusion is the reciprocal of the typical jump frequency (cf. Dingwell, 1990), which is on the order of 10^{-8} s, and therefore closest to the timescale for NMR.

Despite the extensive and detailed information available on silicate liquid structure, there is still considerable uncertainty surrounding the size and lifetimes of polymeric structures in silicate liquids (e.g. Lee and Stebbins, 2006). As noted by Henderson et al. (2006), this "intermediate range structural order, involving organization at nanometer and longer length scales, is still a major challenge but must be of critical importance to kinetics of crystal nucleation and diffusive transport."

1.2. Diffusion in silicate liquids

Diffusion data is usually presented and modeled in terms of simple oxide components, despite the fact that the oxides cannot be the actual diffusing entities. There is a substantial literature on diffusion in silicate liquids, but in particular Dingwell and Webb (1989), Dingwell (1990, 2006), Kress and Ghiorso (1993) and Chakraborty et al. (1995) address the relationships between melt structure or speciation and diffusion. More often, chemical changes due to diffusion are regarded as the result of transport of either oxide or elemental species.

In many cases it is difficult to use diffusion data to infer the existence or composition of multi-atom complexes in silicate liquids. Our approach concerns the effect of diffusion on isotopic fractionation of the major elements of silicate liquids. The only significant difference between isotopes (e.g. ^{44}Ca and ^{40}Ca) is mass. Hence if it is observed that there is a difference in the diffusion coefficients of two isotopes of an element, resulting in isotopic fractionation, it is reasonable to infer that this is due to a difference in the mass of the diffusing *species*. Previous studies have shown that chemical diffusion of Ca, Mg, K, Li, and other minor elements in silicate liquids produces isotopic fractionation because lighter isotopes of an element tend to diffuse slightly faster than heavier isotopes (Baker, 1989; Lesher, 1994; Richter et al., 2003). However, there has not been a systematic investigation of the dependence of isotopic fractionation on liquid composition. Our hypothesis is that such an approach might open a new window for understanding diffusion mechanisms in the context of liquid structure and dynamics.

1.3. Mass dependence of diffusivity

There is no general theory that predicts how diffusivity should vary with mass in liquids. In a dilute gas with mean molecular mass M, the kinetic theory model predicts a power law relationship between diffusivity and the reduced mass μ of isotopically distinct species and that the power law exponent is equal to 1/2 (Mills and Harris, 1976):

$$\frac{D_2}{D_1} = \left(\frac{\mu_1}{\mu_2}\right)^{1/2}, \quad \text{where } \mu_i = \frac{m_i M}{m_i + M}. \tag{1}$$

In the limit that $M >> m_i$, this reduces to commonly used square-root of mass law:

$$\frac{D_2}{D_1} = \left(\frac{m_1}{m_2}\right)^{1/2} \tag{2}$$

In the solid-state diffusion literature, Eq. (2) with a power law exponent of 1/2 is used as a reference and the mass dependence on diffusivity is discussed in terms of the strength of the isotope effect E, which is defined as (Schoen 1958)

$$E = \frac{(D_2/D_1) - 1}{(m_1/m_2)^{1/2} - 1} = 2\frac{\ln(D_2/D_1)}{\ln(m_1/m_2)} \quad (3)$$

where $E = 1$ when Eq. (2) is true. The magnitude of deviations from the $m^{-1/2}$ dependence can be used to infer diffusion mechanisms using crystal lattice models (Rothman and Peterson, 1965). In some cases these mechanisms are discussed in terms of the number and masses of other atoms whose motions are correlated with the movement of the atom of interest. This is essentially a description of diffusive coupling and its effect on the isotopes—a concept that should also apply to isotope diffusion in liquids.

In liquid systems, the approach taken in the geochemical sciences is to assume a power law relationship akin to Eq. (2) but generalized as

$$\frac{D_2}{D_1} = \left(\frac{m_1}{m_2}\right)^{\beta} \quad (4)$$

where it is observed that the power law exponent β is always some value less than ½ in aqueous solutions (Richter et al., 2006; Bourg and Sposito, 2007, 2008), and silicate liquids (Richter et al., 1999, 2003, 2008). This is similar to Eq. (3) and one can easily convert between the two through the relationship that $E \approx 2\beta$.

Calculations of E and/or β implicitly assume that a power law relationship exists between diffusivity and mass in condensed systems and that the mass of the diffusing species m_1 is that of the isotope itself. In pure metals, this is perhaps unambiguous, but in silicate liquids it is not. The general interpretation for values of $E < 1$ is that the movement of the atoms of interest (of masses m_1 and m_2) is correlated with the movements of other atoms, and the value of E can be estimated if the number and masses of the other atoms involved are known. Rothman and Peterson (1965) give the following more general expression for E:

$$E' = \frac{2\ln(D_2/D_1)}{\ln[(nm + m_1)/(nm + m_2)]} \quad (5)$$

where m and n are the average mass and the number, respectively, of the other species whose motions are correlated with those of the tracer atoms during diffusion. This general formula can allow one to speculate about whether diffusion involves larger complexes in the liquid phase, and how large those complexes might be. For example, if the motion of Ca were correlated with that of an AlO_4 tetrahedral unit (mass 91), then the ratio of the diffusivities of ^{44}Ca and ^{40}Ca would appear to correspond to masses of 135 and 131 (for $E = 1$) rather than to masses 44 and 40.

1.4. Diffusive isotopic fractionation

Richter et al. (2003) (hereafter RDDW) and Richter et al. (2008) observed isotopic fractionation of Ca, Mg, and Li as a result of interdiffusion between a mid-ocean ridge (tholeiitic) basalt and rhyolite. Using a chemical diffusion model (the significance of this will be addressed later), RDDW determined the ratio of the diffusivities of ^{44}Ca and ^{40}Ca to be $D_{44}/D_{40} = 0.993$, the diffusivities of ^{7}Li and ^{6}Li to be $D_7/D_6 = 0.967$ and the diffusivities of ^{26}Mg and ^{24}Mg to be $D_{26}/D_{24} = 0.996$. The uncertainties on these numbers are not precisely defined, but they are roughly ±0.0015.

Table 1 summarizes the results of the Richter et al. (2003, 2008) experiments on silicate liquids, and includes the values of β, as well as numbers derived from Eq. (5) for the value of $(nm + m_1)^*$, which assumes $E' = 1$ and is therefore a maximum for this parameter. For Ca and Mg, the derived values for $(nm + m_1)^*$ are substantially larger than the atomic mass of the light isotope and suggestive that the movement of these species is correlated with the movement of at least 5–6 other atoms in the liquids. In contrast, the value of $(nm + m_1)^*$ for Li is not much larger than the atomic mass of Li, and in fact requires $n < 1$ if m is to represent the mass of a major element. This suggests that for Li, the diffusing species is probably the Li atom, and its movements are not strongly correlated with the movement of other species in the liquid.

2. APPROACH

If a complex like $CaAl_2O_4$ were important for diffusion, it would imply that diffusion of Ca and Al be strongly coupled. In addition, one might expect that if there are multiple Ca-bearing complexes, each complex should have a different effect on the mass discrimination of Ca during diffusion.

The experiments of Richter et al. (2003, 2008) were done using the same compositions of basalt and rhyolite in all cases. The basalt is a tholeiitic mid-ocean ridge composition and the rhyolite is a calc-alkaline composition (Table 2). As we noted earlier, these experiments provide interesting insights on the possible structure of silicate liquids, and more information may be accessible by varying the compositions of the liquids. For example, more Mg-rich and Al-poor liquids would have fewer Al–Si–O complexes and therefore fewer bridging oxygen atoms between $(Al,Si)O_4$ tetrahedra, which could in turn affect values for $(nm+m_1)^*$ for a given cation.

To test how mass discrimination by diffusion is related to silicate liquid structures, we performed experiments similar to those of Richter et al. (2003, 2008) using different starting compositions for the mafic endmember (Table 2). In our first two experiments, we chose a Hawaiian basalt composition (H36B; Hofmann and Magaritz, 1977) rather than the tholeiitic basalt used by RDDW. In subsequent experiments, we replaced basalt with ugandite (U105), chosen for its lower silica content, lower Al, higher Mg and alkalis, and because it is presumably less polymerized than tholeiitic basalt. As described below, both series of experiments produced Ca isotopic effects that are significantly different from those observed by RDDW.

3. EXPERIMENTAL METHODS AND MEASUREMENTS

Our experimental design is identical to that described in RDDW. Our starting materials are mafic rock powder (Kilauea basalt H36B and ugandite U150) and natural rhyolite glass (Lake County Obsidian, or LCO). These are juxtaposed vertically in a graphite capsule with the

Table 1
Differences in isotope diffusivities for Ca, Mg, and Li obtained in basalt–rhyolite interdiffusion experiments.

Isotopic system	D_2/D_1	β	Reference	$(nm + m_1)$*
$^{44}Ca/^{40}Ca$	0.993	0.075	Richter et al. (2003)	278
$^{26}Mg/^{24}Mg$	0.996	0.05	Richter et al. (2008)	249
$^{7}Li/^{6}Li$	0.967	0.215	Richter et al. (2003)	15

Table 2
Bulk composition and Ca isotope composition of starting materials used in diffusion-couple experiments. Major element abundances are shown both in terms of oxide components as well as in terms of species used in the Bottinga and Weill (1972) viscosity model.

	Storting compositions			
	SUNY MORB* Tholeiitic basalt	H36B** Tholeiitic basalt	U105 (XRF) Ugandite	LCO (WDS) Rhyolite
Weight percent				
SiO_2	49.75	49.68	40.56	75.94
TiO_2	1.63	2.59	5.02	0.11
Al_2O_3	16.07	12.7	8.04	12.89
Fe_2O_3	—	—	—	—
FeO	9.49	11.05	12.21	0.81
MnO	—	0.17	0.20	0.04
MgO	8.56	9.46	11.81	0.11
CaO	10.80	10.79	12.66	0.75
Na_2O	2.89	2.31	2.47	2.96
K_2O	0.18	0.4&	3.71	5.48
P_2O_5	—	—	0.44	—
LOI	—	—	2.13	—
Total	99.37	99.23	99.81	99.09
Mole percent				
$KAlO_2$	0.26	0.67	4.97	7.71
$NaAlO_2$	6.29	4.89	4.98	6.33
$CaAl_2O_4$	7.36	5.39	0	0.87
$MgAl_2O_4$	0	0	0	0.18
SiO_2	55.85	54.22	42.59	83.76
TiO_2	1.38	2.13	3.97	0.09
FeO	8.91	10.09	10.72	0.75
MgO	14.33	15.39	18.49	0
CaO	5.63	7.23	14.23	0
Na_2O	0	0	0.05	0
K_2O	0	0	0	0
$\delta^{44}Ca^{2‡}$	−0.22	−0.33	−0.41	−0.28

* Richter et al. (2003).
** Hofmann and Magaritz (1977).
‡ Uncertainties in $\delta^{44}Ca$ are within ±0.15‰.

mafic endmember below the felsic endmember to ensure gravitational stability. The graphite capsule is then placed in a standard piston–cylinder assembly (see Fig. 1 in RDDW for details on the dimensions and materials used).

Each of our diffusion couples is run at conditions similar to those used for rhyolite–basalt experiment RB-3 in RDDW (see Table 3). In the piston–cylinder, samples are pressurized to about 1 GPa and then heated to 1450 °C at a ramp rate of 150 °C/min. During the ramping step, pressure is monitored and adjusted to 1.0 ± 0.1 Gpa. Samples are held at constant temperature (which is uniform throughout the capsule; see Section 8.3) and pressure for a specified duration (between 12 h and 24 h) and then quenched by turning off the power. The heating and cooling durations are negligible considering the duration of the experiment and diffusivities of the major-element oxides of interest.

After an experiment, the sample is retrieved and sectioned along axis. The diffusion-couple is mounted in epoxy and polished for microprobe analysis. Axis-parallel major-element profiles are measured with a Cameca SX-51 electron microprobe at UC-Berkeley. We use a 15 nA beam current rastered at 12,000× magnification (~12 μm × 9 μm beam dimensions) with an accelerating voltage of 15 kV. To minimize effects of Na and K loss, these elements are measured first at each spot.

After microprobe analysis, diffusion couples are sectioned into wafers using a Bico diamond wafer saw with

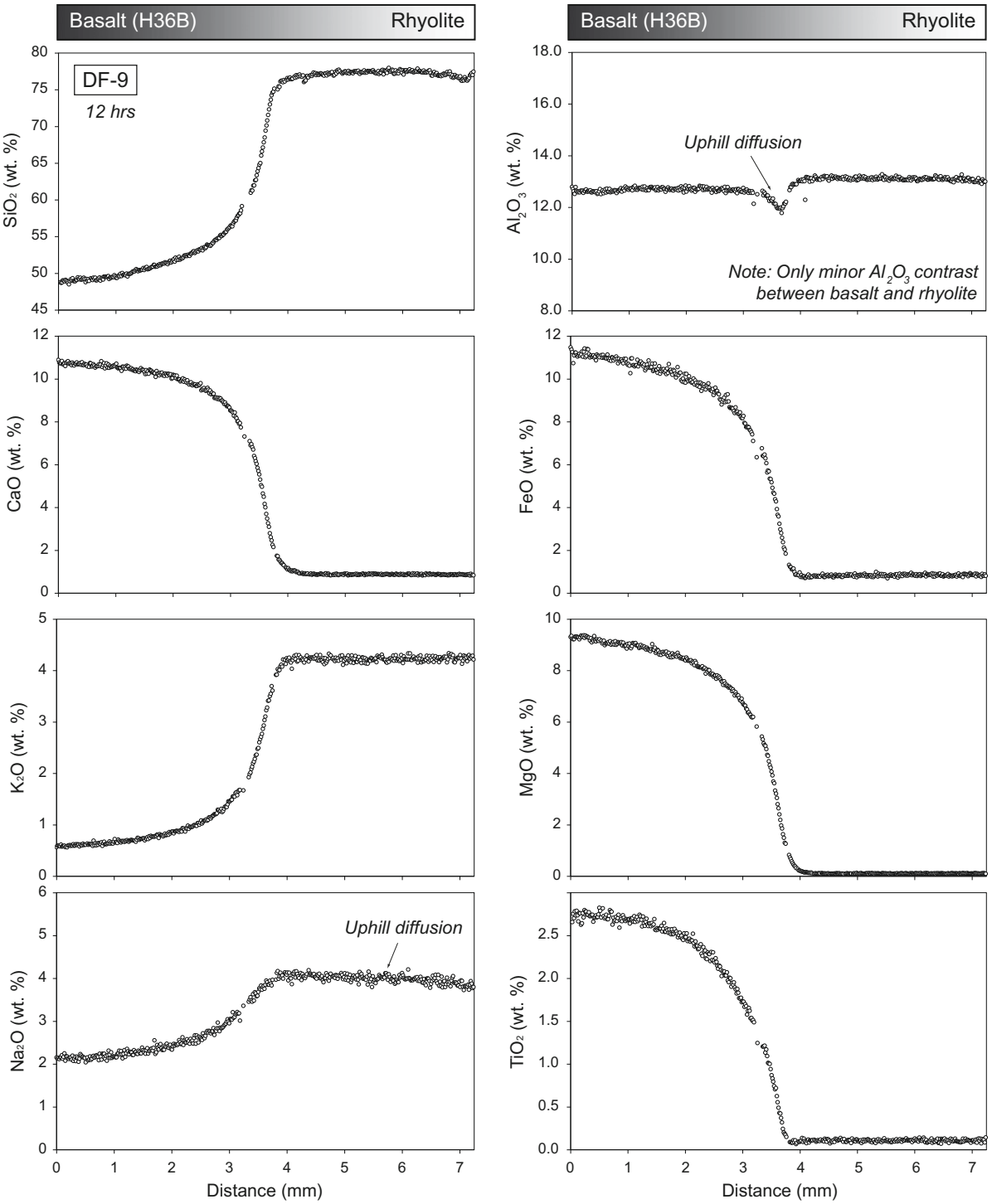

Fig. 1. Major-element diffusion profiles from a basalt–rhyolite diffusion-couple experiment. The asymmetry in each of profile reflects a decrease in diffusivity with increasing silica content. Overall, the profiles are relatively simple, monotonic diffusion profiles except Na_2O and Al_2O_3, which exhibit uphill diffusion. Note the Al_2O_3 contrast between starting liquids is small.

blade thickness of $\sim 165 \pm 2$ μm. Each wafer is $\sim 340 \pm 20$ μm thick and contains enough Ca for at least two Ca isotopic analyses (Ca ~10 μg total in the pure rhyolite wafers). Samples are weighed to high precision ($\sigma \pm 0.00005$ g), though greater uncertainty comes from the fact that weights are affected by residual graphite and/or epoxy on the samples. Sample weight uncertainties do not affect determination of isotopic ratios. Surface contamination from the saw blade and/or environment is addressed by sonicating each wafer in clean isopropyl

Table 3
Initial and experimental conditions for each of the diffusion-couple experiments. RB2 and RB3 are from RDDW. All other experiments were performed in this study.

	Starting compositions		Temperature	Pressure	Duration	Ramp rate	Capsule length (post-run)
	Mafic	Felsic	(°C)	(Gpa)	(h)	(°C/min)	(mm)
RB-2	SUNY MORB	Obsidian	1450	1.3	15.7	75	~8
RB-3	SUNY MORB	Obsidian	1450	1.2	12.0	75	~8
DF-5	Kilauea basalt	Obsidian	1450	1.0	12.0	150	6.98
DF-9	Kilauea basalt	Obsidian	1450	1.0	12.0	150	7.25
DF-8	Ugandite	Obsidian	1450	1.0	24.0	150	8.4
DF-11	Ugandite	Obsidian	1450	1.0	12.0	150	7.12

alcohol, followed by 1.5 N nitric acid, followed by two rinses of ultrapure water. Samples are dissolved in a mixture of concentrated hydrofluoric and perchloric acids in an approximate ratio of 4:1. Dissolved solutions are dried in a perchloric hood and then redissolved in 1.0 N nitric acid. An appropriate amount of ^{42}Ca- and ^{48}Ca-enriched double spike is added to each sample to allow for corrections for mass discriminations produced within the mass spectrometer itself (for a detailed discussion of the double-spike approach, see Johnson and Beard, 1999). The dissolved sample-spike mixtures are loaded onto cation exchange columns and eluted with 1.0 N and 1.5 N nitric acid in order to separate Ca from other major cations. About 3 μg of purified Ca from each sample are loaded onto a zone-refined Re filament to be introduced into the mass spectrometer.

Ca isotope ratio measurements are carried out by thermal ionization mass spectrometry (TIMS) at UC-Berkeley on a Thermo-Finnigan Triton TI with nine moveable Faraday collectors. For each sample, 200 isotope ratio measurements are made in order to reduce within-run uncertainties to about ±0.04‰. For considerations regarding beam intensities and corrections for machine mass discrimination, see DePaolo (2004).

The measured ratios from the mass spectrometer are for the spike–sample mixture. The actual sample isotope ratios are determined using an iterative spike–subtraction algorithm. The algorithm we use is summarized in DePaolo (2004) and shown explicitly for Fe isotopes (analogous to Ca isotopes) in Fantle (2005).

Ca isotope ratios are reported as

$$\delta^{44}Ca = \left[\frac{(^{44}Ca/^{44}Ca)_{sample}}{(^{44}Ca^{40}Ca)_{std}} - 1\right] \times 1000$$

where $(^{44}Ca/^{44}Ca)_{std} = 0.0212076$ (Skulan et al., 1997).

4. RESULTS

A total of four diffusion-couple experiments were measured for chemical diffusion profiles by electron microprobe and sectioned for Ca isotope analysis. Here, we compare and contrast major-element profiles and Ca isotope measurements between the basalt–rhyolite experiments in RDDW, two basalt–rhyolite experiments from this study, and two ugandite–rhyolite experiments from this study. The bulk composition and Ca isotope composition for each starting material is shown in Table 2.

4.1. Major-element diffusion profiles

Figs. 1 and 2 are major-element diffusion profiles for the basalt–rhyolite and ugandite–rhyolite experiments, respectively. All of the profiles exhibit asymmetry that comes from the dependence of diffusivities on composition (primarily silica content). In Fig. 1 there is so-called "uphill diffusion" (i.e., diffusion of a species against its own concentration gradient) exhibited by Na_2O and Al_2O_3, the latter having only a minor concentration contrast between starting materials. The rest of the oxides show generally simple monotonic diffusion profiles. The concentration profiles for the Kilauea basalt–rhyolite experiment are similar to those measured by RDDW in their basalt–rhyolite experiments.

Several of the profiles from the ugandite–rhyolite experiment (Fig. 2) differ markedly from those in the basalt experiment. For instance, there is strong uphill diffusion and/or sharp gradients exhibited by each of the oxides associated with feldspar formula units (K_2O, Na_2O, SiO_2 and Al_2O_3). An inset in the CaO profile shows that CaO also exhibits uphill diffusion. Note that unlike the basalt experiments there is a relatively large Al_2O_3 concentration gradient that is *opposite* the gradient of CaO.

4.2. Calcium isotope profiles

Post-run Ca isotope profiles were measured across each diffusion-couple and large fractionations from the initial Ca isotope composition were observed for each experiment. All Ca measurements are reported in Table 4. Figs. 3a and b show the Ca isotope profiles and corresponding Ca diffusion profiles from RDDW. In their two experiments (RB2 and RB3) the minimum in δ^{44}Ca is about −5 to −6‰ lower than the starting compositions, and the isotopic effects extend nearly to the end of the capsule on the rhyolite side. For comparison, Figs. 3c and d show results from this study for our Kilauea basalt–rhyolite diffusion couples run under the same conditions but with a different, yet still tholeiitic, basalt composition. Overall, the profile has a similar shape, but the minimum δ^{44}Ca is less extreme at −3‰. In addition, our experiments were loaded with a thicker section of rhyolite and it can be seen that the Ca isotopic composition is uniform throughout the rhyolite end of the charge where the rhyolite Ca concentration has been unaffected by diffusion of Ca from the basalt.

Figs. 3e and f show results from ugandite–rhyolite experiments run for 12-h and 24-h, respectively. In these

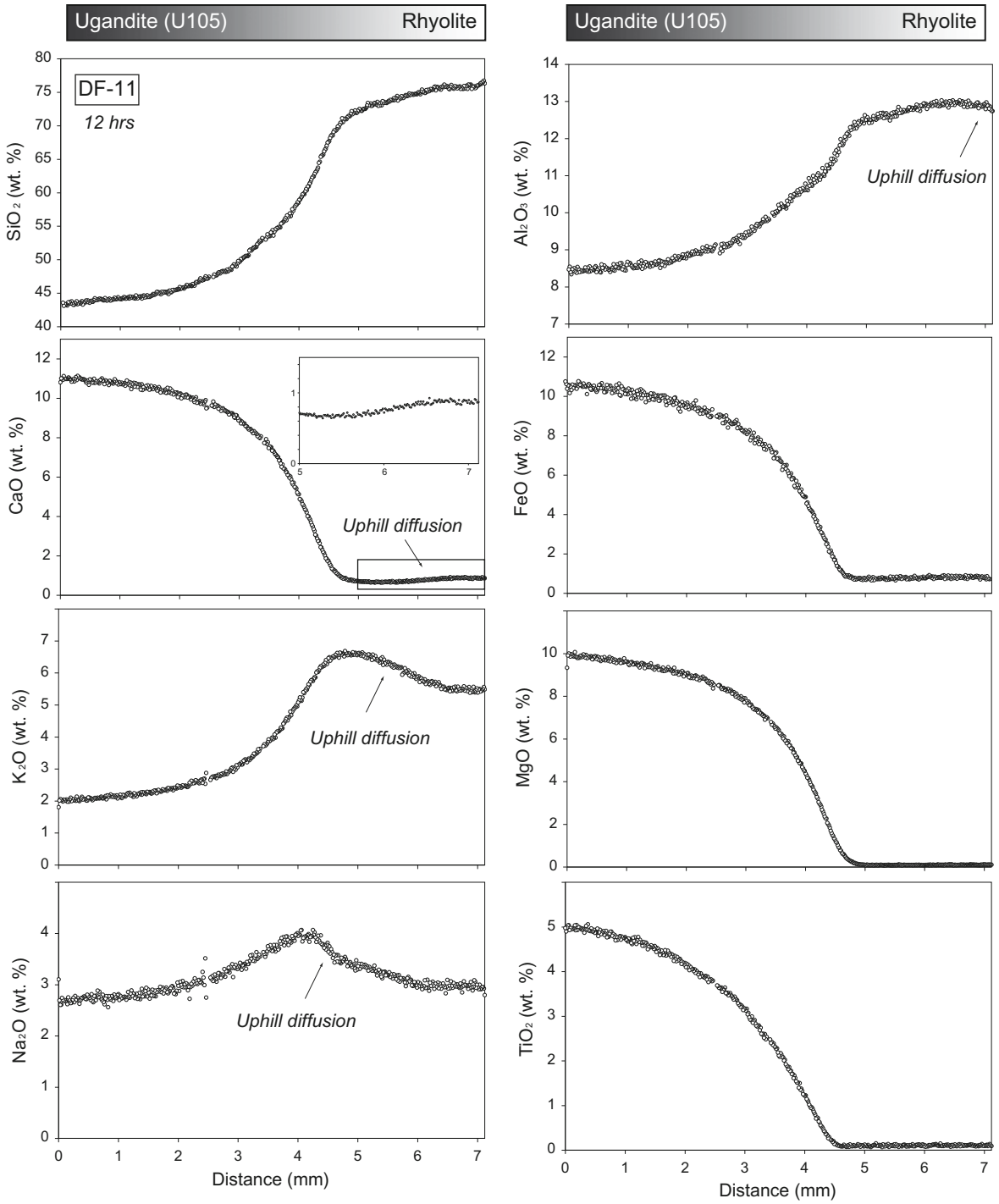

Fig. 2. Major-element diffusion profiles from a ugandite–rhyolite diffusion-couple experiment. Overall, the profiles are more complicated than those in Fig. 1, with uphill diffusion of Na_2O, K_2O, and CaO (see inset) due to, presumably, diffusive coupling to Al_2O_3. Note that unlike the basalt–rhyolite experiments, there is a large Al_2O_3 gradient going from right to left.

experiments, the minimum in $\delta^{44}Ca$ is only about $-2‰$. There is also a large increase in $\delta^{44}Ca$ that developed on the *rhyolite side* of the capsule beyond the diffusion front of Ca from the ugandite. In the 24-h run (Fig. 3f), the increased $\delta^{44}Ca$ extends to the end of the capsule. In all of the experiments, there are linear gradients in $\delta^{44}Ca$ on the mafic side of the capsule with a total range of about 2–4 ‰. A similar linear gradient is observed in one of the RDDW runs (RB-2), and in a run where Mg isotopes were measured (Richter et al., 2008).

Table 4
Ca isotope measurements measured on wafers from four diffusion-couple experiments. Each measurement is an average of 2, 3, or 4 mass spectrometer runs. Also shown are the distances along the Ca diffusion profile associated with the center point of each wafer. Uncertainties in $\delta^{44}Ca$ are within ±0.15‰.

Basalt–Rhyolite experiments			Ugandite–Rhyolite experiments		
Sample (Wafer No.)	Distance (mm)	$\delta^{44}Ca$ (‰)	Sample (Wafer No.)	Distance (mm)	$\delta^{44}Ca$ (‰)
DF5-1	6.727	—	DF8-1	8.153	—
DF5-2	6.229	−0.34	DF8-2	7.659	2.20
DF5-3	5.730	−0.29	DF8-3	7.165	1.94
DF5-4	5.232	−0.19	DF8-4	6.671	0.31
DF5-5	4.734	—	DF8-5	6.176	−1.86
DF5-6	4.235	−2.16	DF8-6	5.682	−1.74
DF5-7	3.737	−2.64	DF8-7	5.188	−1.35
DF5-8	3.239	−2.47	DF8-8	4.694	−1.27
DF5-9	2.741	−1.50	DF8-9	4.200	−1.12
DF5-10	2.242	−1.39	DF8-10	3.706	−1.07
DF5-11	1.744	—	DF8-11	3.212	–
DF5-12	1.246	—	DF8-12	2.718	−0.79
DF5-13	0.747	0.71	DF8-13	2.224	—
DF5-14	0.249	1.25	DF8-14	1.729	−0.16
			DF8-15	1.235	0.15
DF9-1	7.005	—	DF8-16	0.741	—
DF9-2	6.525	−0.24	DF8 17	0.247	—
DF9-3	6.042	−0.49			
DF9-4	5.558	−0.26	DF11-1	6.865	−0.29
DF9-5	5.075	−0.39	DF11-2	6.357	0.25
DF9-6	4.592	−1.99	DF11-3	5.848	1.74
DF9-7	4.108	−2.83	DF 11-4	5.340	1.51
DF9-8	3.625	−1.42	DF11-5	4.831	−0.87
DF9-9	3.138	—	DF11-6	4.323	−2.00
DF9-10	2.658	−0.90	DF11-7	3.814	−1.56
DF9-11	2.175	−0.68	DF11-8	3.305	−1.20
DF9-12	1.692	−0.14	DF11-9	2.797	−0.85
DF9-13	1.208	−0.14	DF11-10	2.288	−0.59
DF9-14	0.725	0.26	DF11-11	1.780	−0.85
DF9-15	0.242	0.76	DF11-12	1.271	—
			DF11-13	0 763	0 17
			DF11-14	0.254	0.23

5. DISCUSSION

5.1. Interpretation of results from basalt–rhyolite experiments

In all of the experiments, isotopes of calcium become fractionated by chemical diffusion as the lighter isotope (^{40}Ca) diffuses slightly faster than the heavy isotope (^{44}Ca). In the basalt–rhyolite experiments, this explains the main features of the measured profiles: (1) Ca has diffused from the basalt end, leaving the basalt isotopically heavier (2) the isotopic composition at the rhyolite end is unchanged because Ca has not diffused into or out of that region, and (3) the isotopic effects are enhanced on the rhyolite side because the rhyolite initially has very little Ca. In the simplest model to describe the diffusion effects (used by RDDW), the minimum in $\delta^{44}Ca$ should depend only on the initial Ca concentration contrast and the relative diffusivities of the isotopes (i.e., β in Eq. (4)).

In the first study of this type, Richter et al. (1999) measured diffusive isotope fractionations of Ca between "synthetic" basalt and synthetic rhyolite and found a value for β of between 0.05 and 0.08. Because those values are similar to the values deduced from the natural basalt–rhyolite experiments in RDDW, it was suggested that $\beta = 0.075$ (±0.025) may be a general feature of silicate liquids, independent of liquid composition. However, in our basalt–rhyolite experiments (Figs. 3c and d), the minimum $\delta^{44}Ca$ of −3‰ translates to $\beta = 0.035 \pm 0.005$, which is significantly different. This result suggests that the relative Ca isotope diffusivities are sensitive to slight changes in liquid composition.

One notable difference between the SUNY MORB and H36B starting materials is in the Al content. In RB2 and RB3, the basalt has a higher concentration of Al_2O_3 than the rhyolite, so the Al concentration gradient between the basalt and the rhyolite (Table 2) is in the same direction as the CaO concentration gradient. In DF5 and DF9, the Al_2O_3 concentration gradient between the basalt and rhyolite is negligible (Fig. 1). This difference is noteworthy since previous studies (e.g., Kubicki et al., 1990; Chakraborty et al., 1995; Liang et al., 1996; and many others)

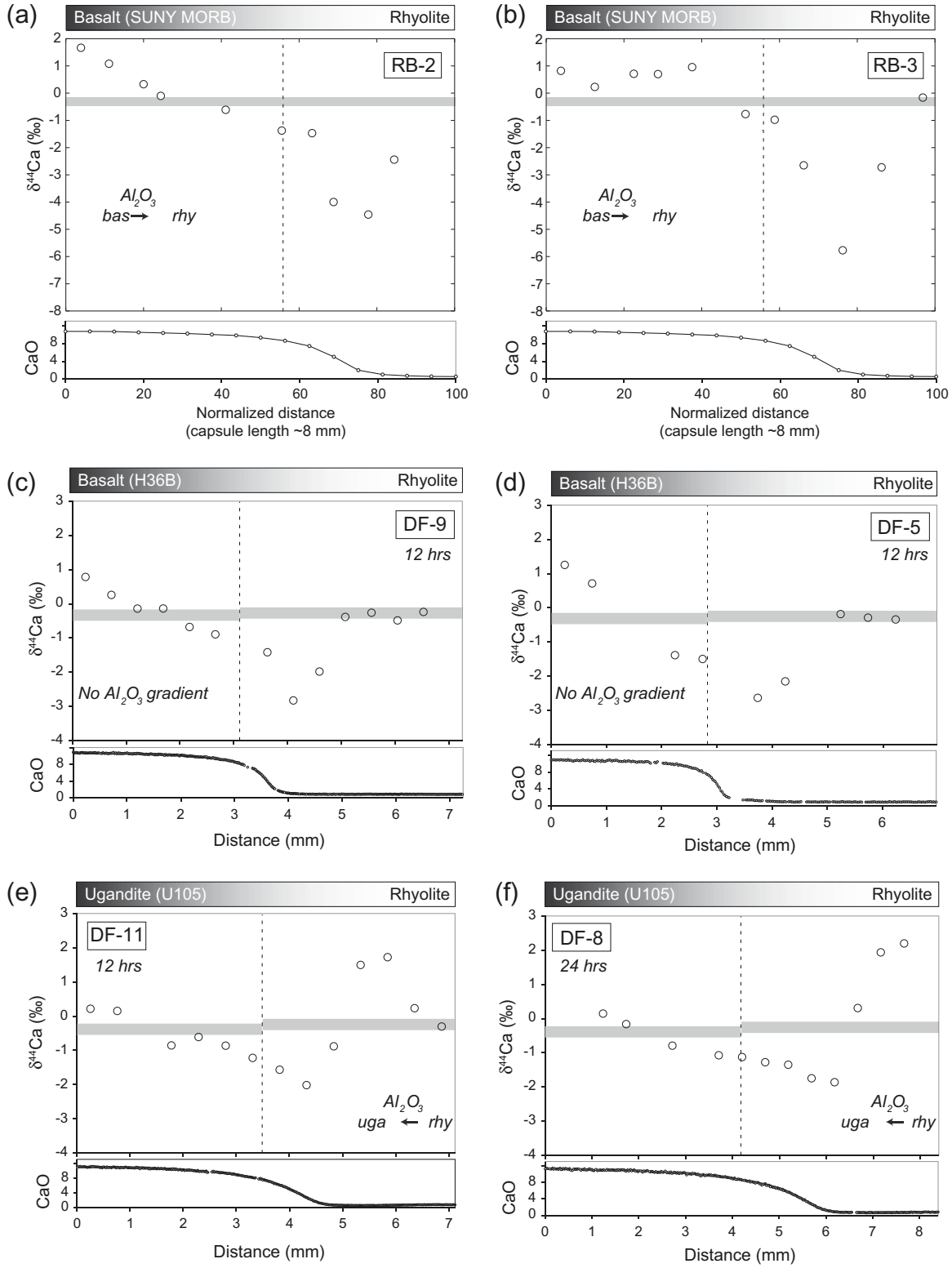

Fig. 3. Ca isotope profiles from three sets of experiments. The initial interface between starting liquids is given by the vertical dashed line. The grey horizontal bar shows the initial isotopic composition. Corresponding CaO diffusion profiles are shown below each plot. The high values of $\delta^{44}Ca$ in the rhyolite in (e) and (f) is interpreted as evidence for diffusive coupling of Ca to Al (see text).

have shown that diffusion of alkali and alkaline-earth cations can be strongly influenced by the magnitude and sign of Al gradients (hereafter referred to as "diffusive coupling").

5.2. Interpretation of results from ugandite–rhyolite experiments

The Ca isotope profiles in the ugandite–rhyolite experiments (Fig. 3e and f) are quite different from those in the basalt–rhyolite experiments. Especially notable is that the ugandite is Al-poor, hence the Al_2O_3 gradient in the ugandite–rhyolite experiments is such that Al is expected to be diffusing from the rhyolite into the ugandite. In these experiments, then, the Al gradient is opposite the Ca gradient, so if Ca and Al are coupled in the diffusion process this might be expected to be evident in the isotopic profiles.

The diffusion-couple produced Ca concentration and isotope profiles on the mafic side of the capsule that are roughly similar to those produced in the Kilauea basalt–rhyolite couples. This requires that Ca is diffusing from the ugandite to the rhyolite, and that the ^{40}Ca species is diffusing more rapidly than the ^{44}Ca species. However, on the rhyolite side of the capsule there are two additional features. A small Ca concentration gradient developed within the rhyolite, with the concentration decreasing *toward* the ugandite. And in the region where this concentration gradient exists, there is a large increase in $\delta^{44}Ca$, suggesting that this region has been depleted of ^{40}Ca by preferential diffusion of light Ca toward the ugandite.

The immediate question is why Ca diffuses from the rhyolite toward the ugandite even though the ugandite has a higher Ca concentration. There are at least two possibilities. Since Ca will diffuse in response to chemical potential gradients, it is possible that Ca has a particularly low chemical potential in the new liquid composition generated within the rhyolite as it diffusively mixes with the ugandite. This might cause Ca to diffuse out of the pure rhyolite into the hybrid composition, depleting the neighboring part of the pure rhyolite in ^{40}Ca relative to ^{44}Ca. An alternative (or additional) explanation is that Al, which is diffusing from the rhyolite toward the ugandite, is combined with Ca in a Ca–Al complex, and that this component or species is diffusing out of the rhyolite toward the ugandite, leaving behind a residue that is enriched in ^{44}Ca. In the latter scenario, it would be required that the ugandite have a lower concentration of the Ca–Al complex than does the rhyolite, and that there is enhanced isotopic discrimination associated with diffusion of the Ca–Al complex.

An observation that seems to suggest the latter explanation is shown in Fig. 4. The minimum $\delta^{44}Ca$ generated in the experiments is correlated with the size and sign of the Al_2O_3 gradient in the diffusion couples. Independent of the mechanism, this result leads to the somewhat surprising conclusion that Ca diffusion in silicate liquids, and in particular the isotopic fractionation effects associated with it, are dependent not only on Ca concentration gradients, but also on Al concentration gradients. It is unclear, however, whether this Ca–Al coupling arises from thermodynamic effects (i.e., the chemical potential of Ca depends significantly on the concentration of Al) or kinetic effects (i.e., motion of Ca is significantly correlated with motion of Al as might be envisioned if the actual diffusing species is a Ca–Al complex). Although we may not be able to distinguish between the two possibilities, the results presented here clearly indicate that diffusive isotopic fractionations of Ca depend on the associations between different elements in the liquid.

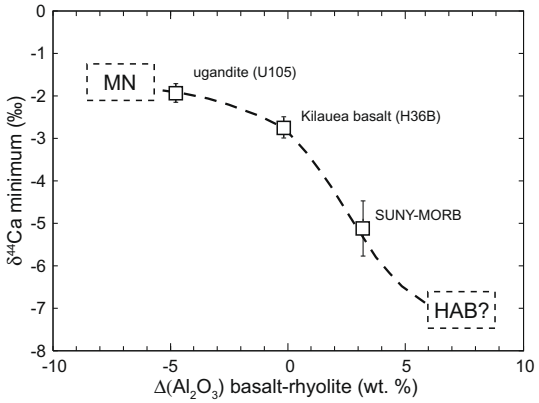

Fig. 4. Correlation between the initial difference in Al_2O_3 between basalt (or ugandite) and rhyolite, and the minimum $\delta^{44}Ca$ observed in the diffusion-couple. Also shown are extrapolated (i.e., guessed) values for other mafic compositions HAB (high-alumina basalt) and MN (olivine melilite).

5.3. Diffusive isotopic fractionation and speciation

There is no general agreement about what long-lived multi-atom species exist in silicate liquids. Empirical viscosity models (e.g., Bottinga and Weill, 1972; Hui and Zhang, 2007) incorporate alkali and alkaline earth aluminate components in addition to the simple oxides in order to account for the dual role of Al as a network-forming and network-modifying cation. Since viscosity and structural relaxation are functionally related to the diffusion of individual atoms in the liquid matrix (Dingwell, 2006), we have chosen to evaluate the possible role(s) that aluminate complexes might play in the diffusion process by recasting the diffusion profiles in terms of the species employed in the viscosity model of Bottinga and Weill (1972), which incorporates two Ca-bearing species, one of which is associated with Al.

Fig. 5 compares the profiles of the two Ca-bearing species (CaO and $CaAl_2O_4$) to the isotope data presented in Fig. 3. In the basalt runs (Fig. 5a and b), the profiles for both Ca species appear to be simple monotonic diffusion profiles. The $CaAl_2O_4$ profile appears to extend further into the rhyolite and suggests that Ca may be more mobile when associated with Al. Fig. 5c and d show CaO and $CaAl_2O_4$ for the ugandite experiments. In these experiments the CaO profile is again monotonic, but exhibits an irregularity in the tail of the diffusion profile that extends to approximately the point where the highest $\delta^{44}Ca$ value lies. The ugandite initially has zero $CaAl_2O_4$ due to its low Al_2O_3 concentration (Table 2), whereas the rhyolite has about 1 mol%. At the end of the run, the $CaAl_2O_4$ profile has become quite complicated. The ugandite near the end of the capsule has acquired $CaAl_2O_4$, and in the mixing region between the liquids, the $CaAl_2O_4$ content is zero. The calculated zero value for $CaAl_2O_4$ arises because the liquids in this region have insufficient Al to make $CaAl_2O_4$ after the

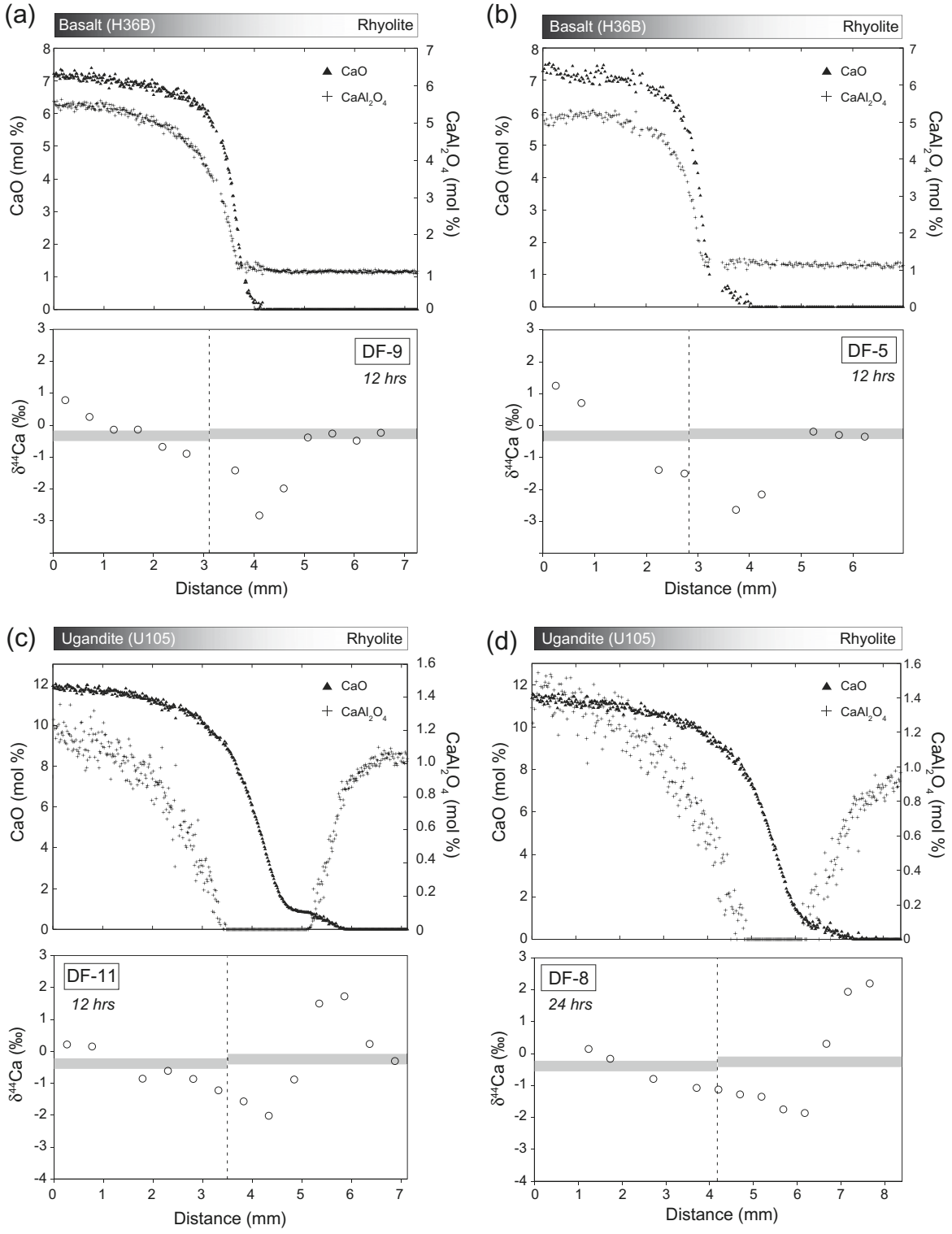

Fig. 5. Major-element profiles from each of the diffusion-couple experiments cast in terms components used in the Bottinga and Weill (1972) viscosity model. The post-run profiles for CaO and $CaAl_2O_4$ are compared to the Ca isotope profiles presented in Fig. 3. In the basalt–rhyolite experiments (a,b), the gradients in both Ca species are unidirectional whereas in the ugandite–rhyolite experiments, there are gradients in Ca species in both directions.

available Al has first been assigned to $KAlO_4$ and $NaAlO_4$. This probably occurs because this region has acquired additional Na_2O and K_2O due to uphill diffusion (Fig. 2). It could reasonably be inferred that in this region, the

chemical potential of the $CaAl_2O_4$ component is very low. The increased values of $CaAl_2O_4$ in the ugandite indicate that Al has been added in excess of any additions of Na and K, which is consistent with the Al_2O_3 profile having penetrated all the way through the ugandite to the end of the capsule (Fig. 2).

Another point is that although the $CaAl_2O_4$ profiles are complicated in these snapshots, the post-run gradients for the 12-h run (Fig. 5c) are similar in sign and shape to those in the 24-h run (Fig. 5d). Hence it appears that these gradients, once established, are maintained throughout the experiments and could be interpreted as indicative of long-lived chemical potential gradients. A further significant feature is the large magnitude of the Ca isotopic effects, in comparison with the magnitude of the Ca and Al gradients, on the rhyolite side of the experiment. This hints that isotopic discrimination may be more pronounced in high-SiO_2 liquids than in low-SiO_2 liquids.

Overall the chemical data suggest that there could be both thermodynamic effects and simple coupling via a Ca–Al complex in the ugandite–rhyolite experiments. The contrasting behavior of the CaO and $CaAl_2O_4$ components in this experiment suggests that two separate Ca-bearing species are diffusing against each other in the liquid. In the following section we pursue the model of counter diffusion of two Ca species to evaluate how well that model can account for the isotopic results.

6. THEORETICAL CONSIDERATIONS

6.1. General multicomponent diffusion model

The mass conservation equation for the chemical diffusion problem is given by

$$\frac{\partial C_i}{\partial t} = -\nabla J_i \tag{6}$$

where J_i is the molar flux of component i (moles cm^{-2} s^{-1}) and C_i is the molar concentration (moles cm^{-3}). In a system of multiple diffusing components, the flux of one component may influence the flux of another and Fick's first law can be expressed as

$$J_i = -\sum_{j=1}^{n-1} D_{ij} \nabla C_j \tag{7}$$

where D_{ij} is the multicomponent diffusion matrix. If diffusion of each component i is independent of all other components, then D_{ij} is a diagonal matrix. Generally, this is not the case in natural silicate liquids when individual elements or oxides are taken as the components, and the off-diagonal elements of D_{ij} specify the extent of diffusive coupling between these components.

If the diagonal or off-diagonal diffusion coefficients for a given element are mass dependent, then the flux of isotope k of element i can be written as (Liang, 1994 and Richter et al., 1999):

$$J_{ik} = -D_k \nabla C_{ik} - \sum_{j=1}^{n-1} \chi_{ij}(D_{ij} - \delta_{ij} D_k) \nabla C_j \tag{8}$$

Where D_k is the self-diffusion coefficient of isotope k, C_{ik} is the concentration of k, and χ_{ik} is the mole fraction of k in element i. Eqs. (2) and (4) lead to the multicomponent diffusion equation with isotopes:

$$\frac{dC_j}{dt} = -\nabla(D_k \nabla C_{ik}) + \sum_{j=1}^{n-1} \nabla(\chi_{ik}(D_{ij} - \delta_{ij} D_k) \nabla C_j) \tag{9}$$

For our experiments, the appropriate boundary conditions are of zero flux into or out of either end of the capsule:

$$J_i = 0 \quad \text{at } x = 0 \quad \text{and } x = L \tag{10}$$

Solving Eq. (9) requires knowledge of the diffusion matrix, which must be determined experimentally for a given composition (cf. Trial and Spera, 1994). Not only is D_{ij} not known for natural basalt or rhyolite, but D_{ij} is sensitive to composition between these two endmembers. Furthermore, because natural melts contain 8–12 oxide components, D_{ij} becomes prohibitively large to be forward-modeled. Therefore, implementing a full multicomponent diffusion model that includes coupling between all major oxides is not practical. However, the essential behavior resulting from the coupling can be captured in a simplified model.

6.2. Simplified multicomponent diffusion model

Our goal is to obtain diffusion coefficients for Ca in a simplified model that takes into account the important observations that (1) Ca diffusion profiles are asymmetric and (2) that Ca diffuses against its own concentration gradient (assumed to be due to Ca–Al coupling) in the ugandite–rhyolite experiments. In our treatment that follows, we arbitrarily choose the simple oxides as components as is customary and for ease of comparison to other diffusion studies.

Based on qualitative assessment of the measured major-element and Ca isotopic profiles, we assume: (1) the rates of CaO diffusion are dependent mainly on the SiO_2 and Al_2O_3 content of the liquids such that we can treat the three oxides as a three-component system, (2) the diffusivities of SiO_2, Al_2O_3, and CaO are controlled by SiO_2 content as in RDDW, and (3) that CaO fluxes are coupled to Al_2O_3 gradients to allow for uphill diffusion of CaO in the ugandite–rhyolite experiments. The one-dimensional matrix representation of our system of equations is:

$$\begin{bmatrix} \frac{\partial C_{SiO_2}}{\partial t} \\ \frac{\partial C_{Al_2O_3}}{\partial t} \\ \frac{\partial C_{CaO}}{\partial t} \end{bmatrix} = \frac{\partial}{\partial x} \left(\begin{bmatrix} D_{SiO_2} & 0 & 0 \\ 0 & D_{Al_2O_3} & 0 \\ 0 & D_{CaO\text{–}Al_2O_3} & D_{CaO} \end{bmatrix} \begin{bmatrix} \frac{\partial C_{SiO_2}}{\partial x} \\ \frac{\partial C_{Al_2O_3}}{\partial X} \\ \frac{\partial C_{CaO}}{\partial x} \end{bmatrix} \right) \tag{11}$$

Note that the diffusion matrix is asymmetric, which in general is to be expected because of constraints such as local charge conservation; for example, one Ca atom coupled to two Al atoms in a species such as $CaAl_2O_4$. Also note that we allow Ca–Al coupling but not vice versa, and this is solely in order to minimize the number of free parameters (although the effect of Ca on the Al profile should be relatively small in comparison to coupling effects of other cations such as K and Na; Bottinga and Weill 1972).

To reproduce the asymmetry in the measured diffusion profiles, D_{SiO_2}, $D_{Al_2O_3}$, and D_{CaO} have a dependence on SiO_2 content that is parameterized as (RDDW):

$$D_{oxide} = D_{a,oxide}\exp(-\alpha_{oxide}(X_{SiO_2} - 0.5)) + D_{1,oxide} \quad (12)$$

where X_{SiO_2} is the weight fraction of SiO_2 and $D_{o,oxide}$, α, and $D_{1,oxide}$ are fitting parameters for the major-element diffusion profiles. For simplicity, $D_{CaO-Al_2O_3}$ is assumed constant.

Referring to Eq. (9), we allow the diagonal and off-diagonal diffusion coefficients of ^{40}Ca and ^{44}Ca to differ by a constant factor. Expressing this difference in terms of the inverse mass ratio, we have two parameters β and γ defined as:

$$\frac{D_{^{44}CaO}}{D_{^{40}CaO}} = \left(\frac{40}{44}\right)^{\beta} \quad (13)$$

and

$$\frac{D_{^{44}CaO-Al_2O_3}}{D_{^{40}CaO-Al_2O_3}} = \left(\frac{40}{44}\right)^{\gamma} \quad (14)$$

where β is the same as in Eq. (4) and γ describes the effect of diffusive coupling on the isotopes.

7. NUMERICAL CALCULATIONS

All numerical calculations were performed using the lattice Boltzmann (LB) method. The LB method is a statistical approach to solve partial differential equations. It has been developed over the last two decades with a special emphasis on complex fluid dynamics and reaction–diffusion problems (Frisch et al., 1986; Qian et al., 1992; Chopard and Droz, 1998; Succi, 2001). Although LB models have been shown to be generally equivalent to explicit finite difference schemes, the LB diffusion models are unconditionally stable unlike finite difference models.

7.1. Model versus measured oxide profiles

The first step in modeling the major-element diffusion profiles is to obtain a reasonable approximation to the SiO_2 data. This provides the time-evolution of SiO_2, which is necessary for modeling the asymmetric Al_2O_3 and CaO profiles with their SiO_2-dependent diffusivities. After fitting the Al_2O_3 profile, we fit the CaO profile, which depends on the evolving SiO_2 and Al_2O_3 concentrations at each node. Lastly, we obtain parameters for the isotope profiles. To summarize:

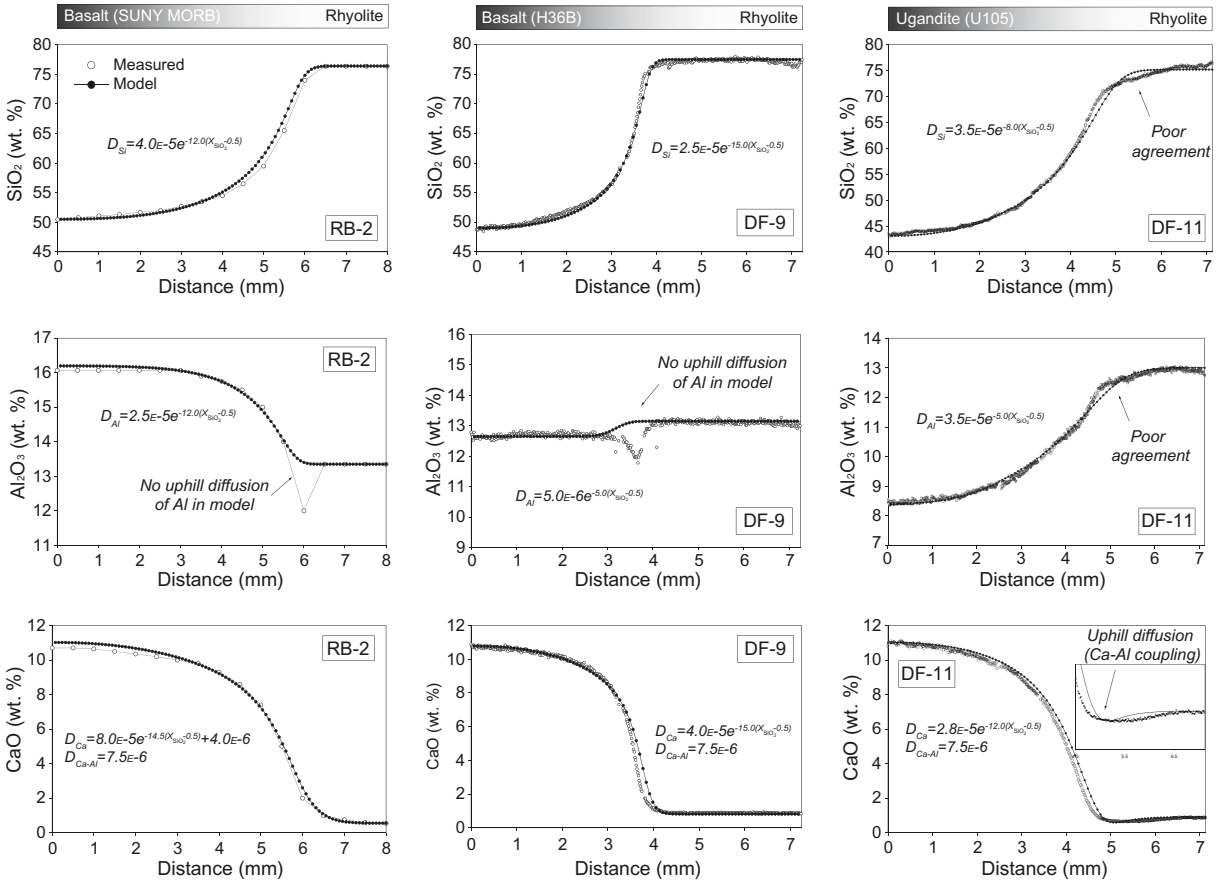

Fig. 6. Model versus measured diffusion profiles for SiO_2, Al_2O_3, and CaO from the three sets of experiments. The model assumes three-component diffusion and includes diffusive coupling of CaO to Al_2O_3. Diffusivity parameters for the model profiles are given in each panel in units of mm^2/s. Despite the relative simplicity of the model, a reasonable fit can be achieved for CaO, which is then used to generate the Ca isotopic profiles in Fig. 7.

(1) Fit SiO_2 data (3 free parameters in D_{SiO_2}).
(2) Fit Al_2O_3 data (3 free parameters in $D_{Al_2O_3}$).
(3) Fit CaO data (3 free parameters in D_{CaO}).
(4) Model the Ca isotope profile (2 free parameters β and γ).

Fig. 6 compares model versus measured SiO_2, Al_2O_3 and CaO diffusion profiles from the three sets of experiments discussed in this paper. The parameters used to model RB2 are the same as those given by RDDW and Fig. 6 shows that our numerical algorithm achieves the same fit for these profiles.

Fig. 6 provides calculated diffusion coefficients and shows that our simplified three-component diffusion model is able to capture the asymmetry and uphill diffusion of CaO in the measured profiles. It is also apparent, however, that our simplifying assumptions result in significant misfit to the data. For example, the model fails to reproduce the uphill diffusion of Al_2O_3 in the basalt–rhyolite experiments because Al_2O_3 fluxes are not coupled to gradients of any other oxides such as Na_2O and K_2O (in this case, coupling Al_2O_3 to CaO would be of little help since the CaO concentration gradients are small in this region). Also, the SiO_2 and Al_2O_3 profiles of DF11 are poorly reproduced where there are unsmooth gradients (i.e., a sharp kink) and uphill diffusion in the rhyolite. The important point, however, is that the model produces the important characteristics of the CaO profiles, including the magnitude of uphill diffusion seen in the ugandite–rhyolite experiment (Fig. 6c). The misfit in the width of the uphill diffusing region can probably be attributed to the misfit in the Al_2O_3 gradients that our model fails to capture.

7.2. Model versus measured Ca isotope profiles

Beginning with the model major-element profiles, we incorporate the isotopic differences (described by β and γ) to produce a model isotopic profile. Fig. 7 compares model versus measured isotopic profiles for the three sets of diffusion couples studied. The model succeeds in capturing the overall shape and parameters can be found to match the magnitude of the observed fractionations in each profile. In both DF9 and DF11, the disagreement between model and data on the rhyolite end may arise from our inability to successfully capture the corresponding gradients in the Al_2O_3 profiles. In all three sets of experiments, our model fails to reproduce the roughly linear isotopic gradients on the mafic end (which we address in Section 8.3).

The simplified multicomponent diffusion model does provide some interesting and useful quantitative results. Using DF9 as a starting point, we find that $\beta = 0.035$ (where γ is poorly constrained because there are essentially no Al_2O_3 gradients). In DF11, where Al_2O_3 gradients are large and opposite the CaO gradients, we can obtain values of $\beta = 0.035$ and $\gamma = 0.075$. Finally, in RB2 and RB3, we find that with diffusive coupling (and assuming $\gamma = 0.075$), we calculate $\beta = 0.035$, which is much different than the value calculated without diffusive coupling (i.e., $\beta = 0.075$; RDDW).

To summarize, we can find a single set of parameters ($\beta = 0.035$ and $\gamma = 0.075$) to describe the fractionations in all of the profiles. We also find that γ is significantly greater than β in the ugandite–rhyolite experiment, implying one or both of the following: (1) diffusive coupling discriminates between isotopes more strongly than simple chemical diffusion or (2) mass discrimination by diffusion is more pronounced in the rhyolite where the coupling effects are being directly observed. We favor the latter interpretation for reasons discussed in the following section.

8. DISCUSSION

Our experiments indicate that the isotopic effects associated with diffusion in silicate liquids are more complicated than has yet been appreciated. Nevertheless, the Ca, Mg, and Li results can be explained in a relatively straightforward manner in terms of two distinct diffusion mechanisms by which cations move.

8.1. Physical explanation for mass discrimination by diffusion

Dingwell (1990) suggested that the diffusive behavior of cations depends on the ratio

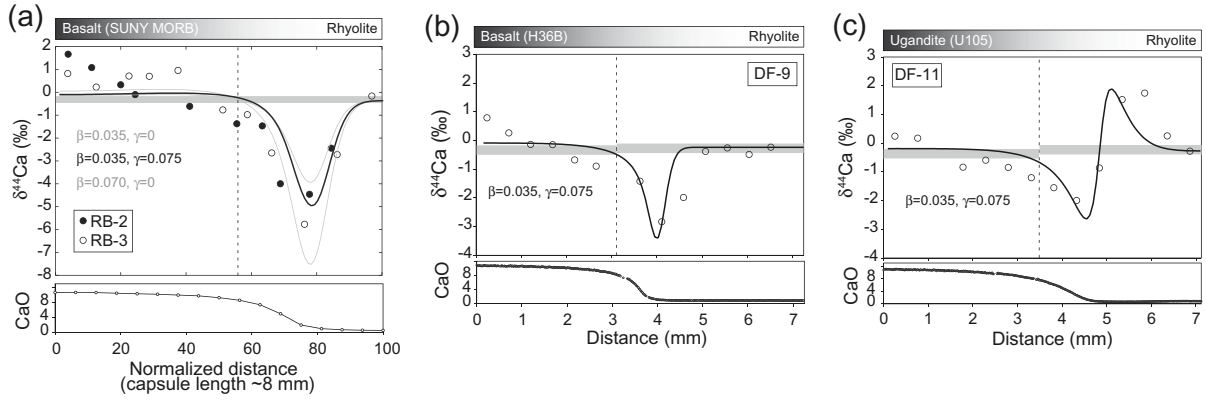

Fig. 7. Model versus measured Ca isotope profiles for the three sets of experiments (labeled a–c). Despite the relative simplicity of the model, the overall shape and magnitude of the fractionations are reproduced. The disagreement between model and data on the rhyolite end of the capsules may be related to the misfit in the same region of the Al_2O_3 profiles in Fig. 6.

$$D_{cation}/D_{Eyring} \quad (15)$$

where D_{cation} is the cation diffusivity and D_{Eyring} is the so-called Eyring diffusivity, which correlates with melt viscosity and is commonly used as a proxy for the mobility of the melt matrix. The Eyring diffusivity can be calculated from (Dingwell, 1990):

$$D_{Eyring} = kT/\lambda\eta \quad (16)$$

where k is Boltzmann's constant, T is temperature (K), λ is an effective jump distance (Dingwell and Webb, 1989), and η is melt viscosity.

Fig. 8 embodies the physical description for cation diffusion described by Dingwell which, we argue, can explain the major features of diffusive isotopic fractionations discussed in this paper. The figure compares D_{Si}, D_{Al}, D_{Ca} and D_{Eyring} versus melt viscosity across the ugandite–rhyolite diffusion-couple. Also shown is D_{Li} from RB5. When D_{cation}/D_{Eyring} is large, as is the case for Li, the cation can be viewed as diffusing by site-hopping within and between quasi-static (glass-like?) structures. This is referred to as the *intrinsic* regime of diffusion (Dingwell, 2006), and in this regime, the diffusion of the species is largely independent of the movements of other atoms or multi-atom structures in the liquid. Consequently, the mass dependence of the diffusivity is closer to the $m^{-1/2}$ dependence (or in other words, the efficiency parameter E in Eq. (3) is relatively large (0.43 for Li), and the parameter n in Eq. (5) approaches zero).

In the other limit, as D_{cation}/D_{Eyring} approaches unity, cation motion is increasingly influenced by the continual rearrangement of the dynamic liquid matrix. This is the *extrinsic* end-member regime of diffusion (Dingwell, 2006), whereby cations not only site-hop among, but also translate with, larger structural units. In this regime E becomes small and nm (Eq. (5)) relatively large. The diffusion of Ca and Mg in basalt is in this extrinsic regime, as evidenced by the low values of $E \approx 0.07$–0.15.

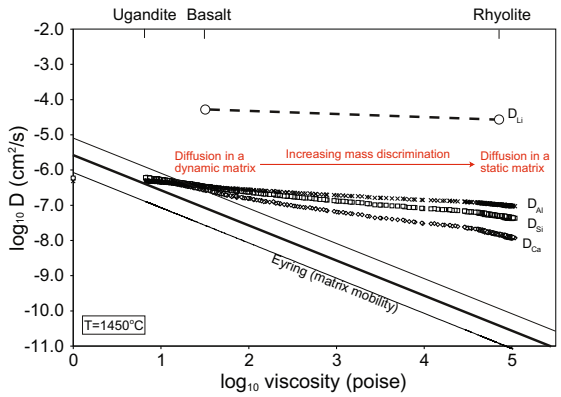

Fig. 8. Diffusivities of Ca, Al, and Si (calculated from our diffusion model) as a function of melt viscosity (calculated using the model of Shaw 1972) across a ugandite–rhyolite diffusion-couple. Also shown are D_{Li} (from RDDW) and D_{Eyring} (using $\lambda = 1.4$ Å, the diameter of an oxygen anion) for the same experimental conditions. The ratio of D_{cation}/D_{Eyring} depends on the cation as well as melt viscosity, which can explain the diffusive isotopic fractionations observed (see text).

We therefore propose that D_{cation}/D_{Eyring} is a proxy for, and is correlated with the efficiency or strength of mass discrimination for isotopes of diffusing cations in silicate liquids. Based on the dependence of D_{cation}/D_{Eyring} on the SiO_2 concentration of the liquid (Fig. 8), mass discrimination by diffusion should increase in going from mafic to felsic liquid. This would help to explain the rather large isotopic effects in the rhyolite end of the ugandite–rhyolite couple.

It has previously been concluded that silicate liquids are not "molecular" liquids in the sense of organic polymers, but instead are dynamic in that viscous flow and diffusion of network-forming cations are dominated by continual making and breaking of bonds instead of molecular mechanisms of motion (Stebbins, 1995). Indeed, any individual bond, let alone a distinct structural unit or complex, probably lasts no longer than 10^{-4}–10^{-5} s under our experimental conditions as evidenced by motional averaging in NMR studies (Stebbins, 1995). Nevertheless, our experiments clearly demonstrate that however transient their existence, the motion of complexes may be important for diffusion. One way to visualize this is by way of analogy to Mg and Li diffusion in aqueous solutions (Richter et al., 2006; Bourg and Sposito, 2007), where there is evidence from molecular dynamics simulations that the magnitude of isotopic discrimination is a function of the lifetime of water molecules in the first hydration shell around the cation. Applying this analogy to silicate liquids, the magnitude of diffusive isotopic fractionations exhibited by a particular cation should depend on the lifetime of its bond to local aluminosilicate structures and the size of those structures.

8.2. Silicate melt structures and diffusing components

Our isotopic results for Ca, which suggest a reinterpretation of the RDDW results as noted earlier, affect the calculated masses $(nm + m_1)^*$ in Table 1. We calculate a value for the on-diagonal terms affecting Ca of $\beta = 0.035$ ($D_2/D_1 = 0.9965$) rather than the value of 0.075 ($D_2/D_1 = 0.993$) proposed by RDDW. Using Eq. (5), this translates into a maximum mass of 598. For the off-diagonal term, the calculated value is $(nm + m_1)^* = 278$. The latter value is equal to, for example, the combined mass of Ca plus at least two $(Al,Si)O_4$ units. This interpretation does not necessarily require that Ca diffusion involve the motion of long-lived Ca-bearing molecular complexes.

There are several additional lines of evidence to support the notion that molecular-scale structures may be important for diffusion in molten silicates. First, measured diffusion coefficients for a given oxide vary widely (an order of magnitude or greater) even in melts of the same SiO_2 content (e.g., Watson 1982). Similar variability can depend on the direction of the oxide concentration gradient (e.g., Van der Laan et al., 1994) or whether the cation is present in major versus trace quantities (Baker 1989; Lesher 1994; Van der Laan et al., 1994). Each of these observations can be anticipated by appealing to diffusion driven by gradients in molecular complexes as opposed to gradients in the oxides. In one study where the choice of molecular components could be reasonably inferred, Kubicki et al. (1990)

performed diffusion-couple experiments using compositions near the diopside–anorthite join and were able to describe most of their data in terms of simple *binary* diffusion using diopside and anorthite as the diffusing components (cf. also Trial and Spera, 1994, who emphasized the significance of this result). Kress and Ghiorso (1993) performed diffusion-couple experiments in the same system (CaO–MgO–Al_2O_3–SiO_2) and found similar results. In both studies, more complicated diffusion behavior arose when the end-member compositions did not lie on the anorthite-diopside join (i.e., one or both of the starting liquids had excess Ca, Mg, Al, or Si). In the latter study, Kress and Ghiorso (1993) attempted to reproduce anomalous features in their diffusion profiles by defining a different set of melt components (from educated guess) and they claim to have found some success using melt species that look like $Mg_2Al_2O_5$ and $MgAl_2Si_2O_8$.

A more quantitative approach for choosing diffusing components would be an eigen component analysis of the full diffusion matrix (cf. Trial and Spera 1994; Chakraborty et al., 1995; and Liang et al., 1996 for discussions and applications of this approach). It has been shown that the full diffusion matrix (which is known for a very limited set of compositions in simplified systems) can be diagonalized (Cullinan 1965) to decouple the set of differential equations describing diffusion. This takes into account all coupling between the oxides by creating new concentration variables (i.e., new components) whose stoichiometry is given by the coefficients in the eigenvectors. Is this approach merely a matter of convenience because the uncoupled set of differential equations are easier to solve (Trial and Spera, 1994) or do the independent components of diffusion have physical meaning in terms of the length scales of interatomic associations that define thermodynamic and/or transport properties? Since the masses we calculate for the diffusing species are comparable in size to common Ca-bearing mineral formula units (which in turn, are comparable in size to thermodynamic components employed in pMELTS; Ghiorso et al., 2002), we speculate that interatomic associations extending about 3–10 Å (corresponding to unit cell dimensions of major minerals) from a central atom correspond to the lengthscales that determine both macroscopic thermodynamic properties (e.g., heat capacity, thermal expansivity, and compressibility) of silicate liquids as well as viscosity and the diffusion behavior of network-modifying cations.

8.3. Thermal gradients in the experiments

In all but one of the experiments shown in Fig. 3, there are linear gradients in $\delta^{44}Ca$ on the mafic side of the diffusion-couple that are unaccounted for in our chemical diffusion model. This issue was addressed by Richter et al. (2008) and it was concluded that these features represent isotope fractionations due to undesired temperature gradients across the sample capsule during the experiments. They supported this conclusion by first assuming that the temperature gradients were restricted to the basalt side; then, they avoided this portion of the furnace by using a shorter basalt–rhyolite diffusion-couple (5 mm instead of 10 mm), and found that the linear isotopic gradients were no longer observed. In a subsequent study aimed at quantifying the ability of thermal gradients to separate isotopes of various elements, Richter et al. (2009) subjected basalt to a large known temperature gradient (about 110 °C) and measured strikingly large Ca isotope fractionations of 6.4‰ per 100 °C between the hot and cold ends of the capsule. From this, one obvious concern is that temperature effects are competing with and overprinting the isotopic effects due to chemical diffusion in our experiments.

To assess the effects of thermal gradients in our experiments, we performed an additional experiment wherein we placed basalt alone in the sample assembly and ran it under exactly the same conditions as all of our previous experiments. Fig. 9 shows the results. We find that although there are isotopic effects that can only be attributed to temperature gradients, these are relatively minor. The total variation in $\delta^{44}Ca$ is about 1.0 ± 0.3‰, corresponding to a temperature difference of $\Delta T = 15 \pm 5$ °C (a value that overlaps with direct measurements by spinel thickness thermometry for the piston–cylinder assembly used by Richter et al., 2009). Fig. 9 also shows that the largest temperature gradients are at the bottom of the capsule (lefthand side of Fig. 9) where the isotopic effects are similar in magnitude to those in the ugandite–rhyolite experiments. However, they are far less pronounced than in the basalt–rhyolite experiments for reasons we do not understand. In Fig. 9, we do not see clear isotopic evidence for temperature gradients near the top of the capsule, in agreement with lack of isotopic gradients in the rhyolite end of each of the basalt–rhyolite experiments (Fig. 3a–d). Richter et al. (2009)

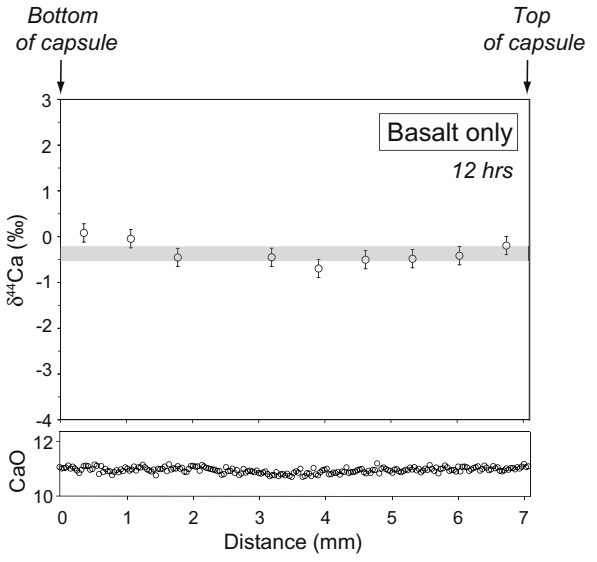

Fig. 9. Results from an experiment to test temperature gradients across the diffusion couples. Basalt was placed in the experimental assembly exactly the way the basalt–rhyolite couples were. The data suggest that a the linear gradients we observe in the mafic end of our diffusion couples can be attributed in part to a temperature gradient of about 15 °C (Richter et al., 2008). There are no discernible isotopic fractionations due to temperature gradients in the top half of the capsules (i.e., the rhyolite end).

modeled the combined chemical and thermal diffusion problem and found that the minimum in $\delta^{44}Ca$ remains unaffected for any reasonable estimate of the temperature distribution in their experiments. Taking this and the observations listed above into account, we conclude that our calculated values for β and γ remain valid as estimates of the mass discrimination by diffusion.

9. SUMMARY AND CONCLUSIONS

We performed superliquidus mafic–felsic diffusion-couple experiments to investigate whether diffusive isotopic fractionations of Ca depend on liquid composition and therefore might be useful to probe silicate liquid structure and dynamics. The results indicate that the ability of chemical diffusion in silicate liquids to fractionate Ca isotopes is dependent on liquid composition, that there may be multiple diffusing Ca-bearing species in silicate liquids, and that these species may be multi-atom complexes that are sufficiently long-lived to affect Ca diffusion behavior. Evidence for strong coupling of Ca diffusion to Al diffusion is provided in two experiments involving a high-Ca, low-Al ugandite composition as the mafic end of the diffusion-couple. The results from the ugandite experiments also suggest that isotopic discrimination by chemical diffusion is stronger in silica-rich, high viscosity liquids than in more silica-poor, low viscosity liquids.

To model the Ca isotope results we used a simplified 3-component diffusion matrix involving Ca-, Al-, and Si-oxides. We find that diffusive isotopic fractionations arise due to a mass-dependence of the diagonal as well as the off-diagonal terms of the diffusion matrix. Hence the isotopic discrimination for Ca isotopes cannot be described in terms of a single parameter, but requires at least two parameters—one being a function of Al concentration. We define two parameters β and γ that quantify the mass dependence of the diagonal and off-diagonal terms, respectively. A single set of β and γ values adequately describes the Ca isotope results from our experiments plus those of Richter et al. (2003), which together involve three different mafic liquid compositions differing mainly in their Al, Na, and K concentrations. Surprisingly, the magnitude of the off-diagonal parameter γ is about twice that of the on-diagonal parameter β. Hence when Al concentration gradients are in the same direction as Ca concentration gradients, Ca isotopic fractionation is enhanced, and when the two gradients are opposed Ca isotopic fractionation is reduced. In addition, an Al concentration gradient can generate Ca isotope fractionation even in the absence of a Ca concentration gradient.

Our results imply that multi-atom molecular complexes may in some instances be the diffusing species in silicate liquids, even though spectroscopic studies indicate that such species have lifetimes that are not much longer than the jump frequency associated with Ca diffusion. This is an intriguing result that needs to be further investigated. The emerging view of silicate liquids from nuclear and vibrational spectroscopy, diffraction studies, and molecular dynamics simulations is that the structure of silicate liquids is constantly changing, with rapid breaking and re-forming of bonds, and a continual rearrangement of species. We reconcile this nanometer-picosecond view of silicate liquids with our results using the Dingwell (1990, 2006) model of extrinsic and intrinsic regimes of diffusion.

Under the experimental conditions ($T = 1450$ °C and $P = 1$ Gpa) fast diffusing cations such as Li diffuse primarily by site-hopping (intrinsic regime) and exhibit large diffusive mass discrimination. Conversely, slower diffusing cations such as Ca and Mg, diffuse by some combination of site-hopping and translating as part of larger structural units (extrinsic regime) and exhibit relatively small diffusive mass discrimination. However, the mass-discrimination for Ca appears to be enhanced in more polymerized liquids. The manner in which cations diffuse through some combination of intrinsic and extrinsic regimes is given by D_{cation}/D_{Eyring}, which is essentially the ratio of the cation jump frequency to the mobility of the melt matrix. Increased polymerization implies a small Eyring diffusivity (and large D_{cation}/D_{Eyring}), which translates to enhanced isotopic fractionations for more polymerized liquids.

The unexpected isotopic fractionation effects described here in mafic–felsic silicate liquid diffusion couples indicate that diffusive isotopic fractionation experiments in both natural and simpler synthetic liquids can provide new information about the way that silicate liquids are structured. The isotopic discrimination effects are complementary to other studies in that they isolate mass-dependent effects from other chemical effects, and they can be studied directly in the liquid state. Results from such studies may help eventually to provide a more comprehensive view of the relationships between atomic and molecular scale processes and macroscopic thermodynamic and transport properties.

ACKNOWLEDGMENTS

We thank Tom Owens and Kent Ross for outstanding technical support with isotopic and microprobe analyses, respectively. This manuscript benefited from discussions with Michael Manga and Mark Ghiorso, and insightful reviews from E.B. Watson, S. Chakraborty, and C. Lesher, and comments from associate editor B. Mysen. J.W. was supported by LLNL IGPP Award #07-GS-008. This material is based upon work supported by the National Science Foundation under Grant Nos. EAR0838168 and EAR0608885. This work was partially performed under the auspices of the U.S. Department of Energy by the University of California, Lawrence Livermore National Laboratory, under Contract Nos. W-7405-Eng-48, DE-AC52-07NA27344, and DE-AC02-05CH1123 (LLNL Report No. LLNL-JRNL-416521). This work was supported by the Director, Office of Science, Office of Basic Energy Sciences, of the U.S. Department of Energy under Contract No. DE-AC02-05CH11231.

REFERENCES

Baker D. (1989) Tracer versus trace element diffusion: diffusional decoupling of Sr concentration from Sr isotope composition. *Geochimica et Cosmochimica Acta* **53**, 3015–3023.

Bourg I. and Sposito G. (2007) Molecular dynamics simulations of kinetic isotope fractionation during the diffusion of ionic species in liquid water. *Geochimica et Cosmochimica Acta* **71**(23), 5583–5589.

Bourg I. and Sposito G. (2008) Isotopic fractionation of noble gases by diffusion in liquid water: molecular dynamics simulations and hydrologic applications. *Geochimica et Cosmochimica Acta* **72**, 2237–2247.

Bottinga W. and Weill D. (1972) The viscosity of magmatic silicate liquids: a model for calculation. *American Journal of Science* **272**, 438–475.

Brown G., Farges F. and Calas G. (1995) X-ray scattering and X-ray spectroscopy studies of silicate melts. *Reviews in Mineralogy and Geochemistry* **32**(1), 317–410.

Calas G., Henderson G. and Stebbins J. (2006) Glasses and melts: linking geochemistry and materials science. *Elements* **2**, 265–268.

Chakraborty S., Dingwell D. and Rubie D. (1995) Multicomponent diffusion in ternary silicate melts in the system K_2O–Al_2O_3–SiO_2: II. Mechanisms, systematics, and geological applications. *Geochimica et Cosmochimica Acta* **59**(2), 265–277.

Chopard B. and Droz M. (1998) *Cellular Automata and Modeling of Physical Systems, Monographs and Texts in Statistical Physics*. Cambridge University Press, 353 p.

Cullinan H. (1965) Analysis of flux equations of multicomponent diffusion. *Industrial and Engineering Fundamentals* **4**(2), 133–139.

DePaolo D. J. (2004) Calcium isotopic variations produced by biological, kinetic, radiogenic and nucleosynthetic processes. *Reviews in Mineralogy and Geochemistry* **55**, 255–288.

Dingwell D. and Webb S. (1989) Structural relaxation in silicate melts and non-Newtonian melt rheology in geologic processes. *Physics and Chemistry of Minerals* **16**, 508–516.

Dingwell D. (1990) Effects of structural relaxation on cationic tracer diffusion in silicate melts. *Chemical Geology* **82**, 209–216.

Dingwell D. (2006) Transport properties of magmas: diffusion and rheology. *Elements* **2**, 281–286.

Fantle M.S., 2005. The global geochemical cycles of iron and calcium: using novel isotope systems to understand weathering, global mass budgets, natural reaction rates, and paleoclimate, Ph.D. dissertation, University of California–Berkeley.

Frisch U., Hasslacher B. and Pomeau Y. (1986) Lattice gas automata for the Navier–Stokes equations. *Physical Review Letters* **56**, 1505–1508.

Ghiorso M., Carmichael I., Rivers M. and Sack R. (1983) The Gibbs free-energy of mixing of natural silicate liquids–an expanded regular solution approximation for the calculation of magmatic intensive variables. *Contributions to Mineralogy and Petrology* **84**(2–3), 107–145.

Ghiorso M., Hirschmann M., Reiners P. and Kress V. (2002) The pMELTS: a revision of MELTS for improved calculation of phase relations and major element partitioning related to partial melting of the mantle to 3 Gpa. *Geochemistry, Geophysics, Geosystems* **3**. doi:10.1029/2001GC000217.

Halter W. and Mysen B. (2004) Melt speciation in the system Na_2O–SiO_2. *Chemical Geology* **213**, 115–123.

Henderson G., Calas G. and Stebbins J. (2006) The structure of silicate glasses and melts. *Elements* **2**, 269–273.

Hess P. (1995) Thermodynamic mixing properties and the structure of silicate melts. *Reviews in Mineralogy and Geochemistry* **32**(1), 147–189.

Hofmann A. and Magaritz M. (1977) Diffusion of Ca, Sr, Ba, and Co in a basalt melt: implications for the geochemistry of the mantle. *Journal of Geophysical Research* **82**, 5432–5440.

Hui H. and Zhang Y. (2007) Toward a general viscosity equation for natural anhydrous and hydrous silicate melts. *Geochimica et Cosmochimica Acta* **71**, 403–416.

Johnson C. and Beard B. (1999) Correction of instrumentally produced mass fractionation during isotopic analysis of Fe by thermal ionization mass spectrometry. *International Journal of Mass Spectrometry* **193**, 87–99.

Kress V. and Ghiorso M. (1993) Multicomponent diffusion in MgO–Al_2O_3–SiO_2 and CaO–MgO–Al_2O_3–SiO_2. *Geochimica et Cosmochimica Acta* **57**, 4453–4466.

Kubicki J., Muncill G. and Lasaga A. (1990) Chemical diffusion in melts on the $CaMgSi_2O_6$–$CaAl_2Si_2O_8$ join under high pressures. *Geochimica et Cosmochimica Acta* **54**, 2709–2715.

Lee S. and Stebbins J. (2006) Disorder and the extent of polymerization in calcium silicate and aluminosilicate glasses: O-17 NMR results and quantum chemical molecular orbital calculations. *Geochimica et Cosmochimica Acta* **70**, 4275–4286.

Lesher C. (1994) Kinetics of Sr and Nd exchange in silicate liquids: theory, experiments, and applications to uphill diffusion, isotopic equilibration, and irreversible mixing of magmas. *Journal of Geophysical Research* **99**(5), 9585–9604.

Liang, Y., 1994. Models and experiments for multicomponent chemical diffusion in molten silicates. PhD. thesis, Univ. Chicago.

Liang Y., Richter F. and Watson E. (1996) Diffusion in silicate melts: II. Multicomponent diffusion in CaO–Al_2O_3–SiO_2 at 1500 °C and 1 Gpa. *Geochimica et Cosmochimica Acta* **60**(24), 5021–5035.

McMillan P. and Wolf G. (1995) Vibrational Spectroscopy of Silicate Liquids. *Reviews in Mineralogy and Geochemistry* **32**(1), 247–315.

Mills R. and Harris K. (1976) The effect of isotopic substitution on diffusion in liquids. *Chemical Society Reviews* **5**, 215–231.

Mysen, B., Richet, P., 2005. Silicate Glasses and Melts: Properties and Structure. Elsevier Press, 544 p.

Navrotsky A., Ziegler D., Oestrike R. and Maniar P. (1989) Calorimetry of silicate melts at 1773 K: measurement of enthalpies of fusion and of mixing in the systems diopside–anorthite–albite and anorthite–forsterite. *Contributions to Mineralogy and Petrology* **101**, 122–130.

Qian Y. H., D'Humières D. and Lallemand P. (1992) Lattice BGK models for the Navier–Stokes equation. *Europhysics Letters* **17**, 479–484.

Richter F., Liang Y. and Davis A. (1999) Isotope fractionation by diffusion in molten oxides. *Geochimica et Cosmochimica Acta* **63**, 2853–2861.

Richter F., Davis A., DePaolo D. and Watson E. (2003) Isotope fractionation by chemical diffusion between molten basalt and rhyolite. *Geochimica et Cosmochimica Acta* **67**, 3905–3923.

Richter F., Mendybaev R., Christensen J., Hutcheon I., Williams R. and Sturchio N. (2006) Kinetic isotope fractionation during diffusion of ionic species in water. *Geochimica et Cosmochimica Acta* **70**(2), 277–289.

Richter F., Watson E., Mendybaev R., Teng F. and Janney P. (2008) Magnesium isotope fractionation in silicate melts by chemical and thermal diffusion. *Geochimica et Cosmochimica Acta* **72**, 206–220.

Richter F., Watson E., Mendybaev R., Dauphas N., Georg B., Watkins J. and Valley J. (2009) Isotopic fractionation of the major elements of molten basalt by chemical and thermal diffusion, 2009. *Geochimica et Cosmochimica Acta* **73**, 4250–4263.

Rothman S. and Peterson N. (1965) Isotope effect and divacancies for self-diffusion in copper. *Physica Status Solidi* **35**(1), 305–312.

Schoen A. (1958) Correlation and the isotope effect for diffusion in crystalline solids. *Physical Review Letters* **1**(4), 138–140.

Skulan J., DePaolo D. and Owens T. (1997) Biological control of calcium isotopic abundances in the global calcium cycle. *Geochimica et Cosmochimica Acta* **61**, 2505–2510.

Stebbins J. (1995) Dynamics and structure of silicate and oxide melts; nuclear magnetic resonance studies. *Reviews in Mineralogy and Geochemistry* **32**(1), 191–246.

Succi S. (2001) *The Lattice Boltzmann Equation for Fluid Dynamics and Beyond*. Oxford University Press, 288 p.

Trial A. and Spera F. (1994) Measuring the multicomponent diffusion matrix: experimental design and data analysis for silicate melts. *Geochimica et Cosmochimica Acta* **58**(18), 3769–3783.

Van der Laan S., Zhang X., Kennedy A. and Wyllie P. (1994) Comparison of element and isotope diffusion of K and Ca in multicomponent silicate melts. *Earth and Planetary Science Letters* **123**, 155–166.

Watson E. (1982) Basalt contamination by continental crust: Some experiments and models. *Contributions to Mineralogy and Petrology* **80**, 83–87.

Associate editor: Bjorn Mysen